

Domain Wall formation from Z_2 spontaneous symmetry breaking/restoration in Scalar-Einstein-Gauss-Bonnet theory

M.A. Krasnov^{a,b}, D.Z. Berkimbayev^c, A. Addazi^{d,e}, Y. Aldabergenov^f, M. Khlopov^g

^aNational Research Nuclear University MEPhI, Moscow, 115409, Russia

^bResearch Institute of Physics, Southern Federal University, Rostov-on-Don, 344090, Russia

^cAl-Farabi Kazakh National University, Almaty, 050040, Kazakhstan

^dCenter for Theoretical Physics, College of Physics Science and Technology, Sichuan University, Chengdu, 610065, China

^eLaboratori Nazionali di Frascati INFN, Rome, 344090, Italy

^fDepartment of Physics, Fudan University, Shanghai, 200433, China

^gVirtual Institute of Astroparticle physics, Paris, 75018, France

Abstract

This study offers a detailed analysis of domain wall formation and its cosmological consequences in Einstein-Gauss-Bonnet gravity coupled to a scalar field. A central aspect of the model is the scalar field Lagrangian's ability to spontaneously break and restore its Z_2 discrete symmetry. This spontaneous symmetry breaking is a fundamental prerequisite for topological defect formation. In this context, domain walls arise as kink-like, solitonic solutions that interpolate between the distinct vacuum states of the theory. We perform a detailed numerical analysis of the dynamics of a neutral scalar field non-minimally coupled to the Gauss-Bonnet invariant, exploring its behavior across different cosmological backgrounds. Our results show that coupling to the Gauss-Bonnet term enables the formation of static domain walls with a fixed proper distance within a de Sitter (inflationary) background. Furthermore, we extend our analysis to a radiation-dominated epoch, where we identify that the cosmic expansion causes the "melting" of these domain walls. To assess the potential observational signatures of this scenario, we calculate the predicted spectrum of stochastic gravitational waves generated by the network dynamics using *CosmoLattice* package. We also examine the possible generation of Primordial Black Holes (PBHs) associated with collapsing domain walls. Regrettably, our calculations indicate that the direct observational detection of such domain walls from this model lies beyond the reach of foreseeable experiments. Our results constitute a No-Go argument against the generation of PBHs as well as of large amplitude GW signals from domain walls in a Scalar-EGB spontaneous symmetry breaking mechanism.

Keywords: Modified gravity, Domain wall, Black hole, Gravitational waves, Scalar field

1. Introduction

General Relativity (GR), elegantly encapsulated in the Einstein-Hilbert action, has stood for over a century as the definitive classical description of gravity. Its predictions, from the perihelion precession of Mercury to the recent observations of Gravitational Waves (GWs) Abbott et al. (2016, 2017), have been resoundingly confirmed. Nevertheless, GR is not a complete theory. It predicts its own breakdown in singularities, it is fundamentally classical, and it offers no fundamental explanation for the dark energy driving cosmic acceleration. These shortcomings motivate the search for modified theories of gravity. Among the most well-motivated extensions is Einstein-Gauss-Bonnet (EGB) gravity Yousaf et al. (2025); Yogesh et al. (2025); Dadhich (2005), which incorporates a specific quadratic curvature term that naturally arises in the low-energy effective action of string theory and avoids pathological ghost instabilities Nojiri et al. (2019); Himmetoglu et al. (2009); Clough et al. (2022). See e.g. Fernandes et al. (2022) and references therein for review of EGB gravity. EGB modification of gravity provides a rich phenomenology Sotiriou and Zhou (2014); Doneva and Yazadjiev (2018); Silva et al. (2018); Kleihaus et al. (2011);

Odintsov and Oikonomou (2020); Kokubu and Harada (2020); Gregory (2011); Ghosh and Kumar (2020). In addition, this particular extension of GR is capable of explaining accelerated cosmological inflation Pinto (2025); Kanti et al. (2015a); Zahoor et al. (2026) and even play a crucial role in baryogenesis Liang et al. (2019). Inflation coupled to GB were also considered in Kanti et al. (2015b); Jiang et al. (2013); Hwang and Noh (2000); Cartier et al. (2001); Hwang and Noh (2005); Guo and Schwarz (2009, 2010b); Koh et al. (2014); Kawai et al. (1998); Kawai and Kim (2019); Yi et al. (2018); Rashidi and Nozari (2020); Kawai and Kim (2021a,b); Kawaguchi and Tsujikawa (2023); Addazi et al. (2024a).

Our aim is to explore the recently demonstrated Gauss-Bonnet symmetry breaking Aldabergenov and Berkimbayev (2025) as a novel mechanism for domain walls formation and study their potential consequences. It is known that, in a class of modified gravity models, domain walls, and the BHs formed from their collapse, can arise even without the direct inclusion of matter fields Nikulin et al. (2022). Possibility of formation of topological defects during inflation was studied in Basu et al. (1991). Moreover, topological defects could be formed via quantum tunneling processes mediated by instantons. The pro-

cess of evolution of domain walls in de Sitter background was studied in several previous works Basu and Vilenkin (1994); Dolgov et al. (2016, 2018); Guerrero et al. (2006); Sasakura (2002).

In this paper, in the framework of EGB gravity, we introduce a Gauss-Bonnet curvature term coupled with a neutral scalar field with polynomial potential. This work establishes the viability of domain wall formation during inflation and examines the evolutionary dynamics of walls generated in the post-inflationary era. Domain walls produced after inflation 'melt' as their tension decays with cosmological time. Similar cases of melting walls were considered in Dankovsky et al. (2024, 2025b,a); Babichev et al. (2023). In contrast to aforementioned previous results, we identify and demonstrate a specific physical mechanism responsible for melting domain wall formation. Furthermore, in our model the wall tension exhibits a significantly stronger time dependence, which produces a distinct imprint on the GW spectrum generated by these walls. In particular, we establish a no-go result, showing that our model cannot generate significant signals of either GWs or PBHs from domain walls. Broadly speaking, we show that the domain walls predicted by our model are effectively invisible, leaving almost no observable signatures in the late Universe.

We also utilize *CosmoLattice* package Figueroa et al. (2021, 2023) to study gravitational waves emitted by these melting domain walls.

The paper is organized as follows: Section II is dedicated to the clarification of considered field theory model, in section III we study domain walls which could take place during cosmological inflation and derive constraints on model's parameters in such a scenario, in section IV we describe our setup for lattice simulations via *CosmoLattice* package, in section V we demonstrate gravitational waves spectrum and derive its dependence on initial parameters of the model, then we finalize with discussion and conclusion.

2. Properties of the model

In this section we will present the EGB gravity model with neutral scalar field, which could provide a possibility of formation of domain walls.

We consider the model described by the following Lagrangian:

$$\mathcal{L} = \sqrt{-g} \left(\frac{R}{2} + g^{\mu\nu} \partial_\mu \phi \partial_\nu \phi - V(\phi) - \frac{1}{8} \xi(\phi) R_{GB}^2 \right) + \mathcal{L}_{inf} + \mathcal{L}_m, \quad (1)$$

where Gauss-Bonnet term R_{GB}^2 is as follows:

$$R_{GB}^2 = R^2 - 4R_{\mu\nu}R^{\mu\nu} + R_{\mu\nu\rho\sigma}R^{\mu\nu\rho\sigma} \quad (2)$$

and $V(\phi)$, $\xi(\phi)$ are given by

$$\xi(\phi) = \frac{1}{2} \alpha \phi^2, \quad V(\phi) = \frac{1}{2} m^2 \phi^2 + \frac{1}{4} \lambda \phi^4. \quad (3)$$

We assume λ to be positive constant, then preservation of Z_2 symmetry is defined by relation between quadratic terms with

their constants α and m . We assume minimal coupling between scalar field ϕ and inflaton field given by Lagrangian \mathcal{L}_{inf} as well as with any other matter fields represented by \mathcal{L}_m .

We also assume Friedmann (FLRW) background, which leads to the following equation of motion of a scalar field:

$$\ddot{\phi} + 3H\dot{\phi} - \nabla^2 \phi + V_\phi + 3\xi_\phi H^2 (\dot{H} + H^2) = 0. \quad (4)$$

The presence of Gauss-Bonnet coupling leads to effective potential of the scalar field to be as follows:

$$V_{eff}(\phi) = V(\phi) + \frac{1}{8} \xi(\phi) R_{GB}^2. \quad (5)$$

In order to have a possibility of stable domain wall formation we need effective potential to possess two equivalent minima, which could be achieved by choosing $\xi(\phi)$, namely, by choosing the value and sign of the coupling constant α . It is of no interest to consider the case of $m^2 < 0$, since this would lead to the well studied in literature case of domain wall production and Gauss-Bonnet term would simply be (qualitatively) irrelevant.

3. Gauss-Bonnet induced domain walls at de Sitter background

In this section we study the possibility of formation of cosmic domain walls in de Sitter background. Such background could be referred to cosmological inflation. We assume that inflaton field or whatever causes background to be de Sitter is an external process, where considered scalar field coupled with Gauss-Bonnet term is subdominant effect.

In works by Vilenkin and Dolgov Basu and Vilenkin (1994); Dolgov et al. (2016, 2018) planar domain walls were studied. In particular, they derived constraints on model parameters, which defines the possibility of stationary wall's structure in terms of proper distance.

Let us consider Eq.(4) in de Sitter background assuming spherical symmetry:

$$\ddot{\phi} + 3H\dot{\phi} - e^{-2Ht} \frac{2\phi_r}{r} - e^{-2Ht} \phi_{rr} + V_\phi + 3\xi_\phi H^4 = 0, \quad (6)$$

which is then rewritten as:

$$\ddot{\phi} + 3H\dot{\phi} - e^{-2Ht} \frac{2\phi_r}{r} - e^{-2Ht} \phi_{rr} + \lambda \phi (\phi^2 - \eta^2) = 0, \quad (7)$$

where $\eta^2 = -\left(\frac{3\alpha H^4 + m^2}{\lambda}\right)$. To have a real positive η it is required that $\alpha < -m^2/3H^4$.

Let us now rewrite Eq.(7), using the following substitutions:

$$u = Hre^{Ht}, \quad \phi(u) = f(u)\eta. \quad (8)$$

Then we obtain:

$$f''(1-u^2) - f' \left(4u - \frac{2}{u} \right) = -\frac{3\alpha H^4 + m^2}{H^2} f(f^2 - 1). \quad (9)$$

We can rewrite it as follows:

$$f''(1-u^2) - f' \left(4u - \frac{2}{u} \right) = 2Cf(f^2 - 1), \quad (10)$$

where

$$2C = -\frac{3\alpha H^4 + m^2}{H^2} \quad (11)$$

to follow the notations introduced in Basu and Vilenkin (1994); Dolgov et al. (2016, 2018). Note that in aforementioned papers it was found that $C > 2$ is required for the possibility of static configuration in terms of proper distance. We solve equation Eq.(10) via the shooting routine since this cannot be solved as a border conditions problem. We use a nonlinear numerical scheme to deal with the stiffness at the origin of the radial coordinate and at the point $u = 1$.

Now we demonstrate a numerical solution of Eq.(10) in Fig. 1.

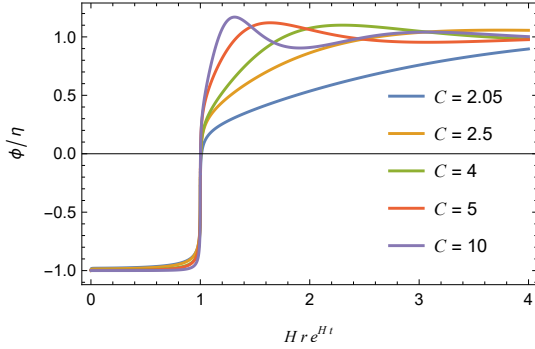


Figure 1: Numerical solution of Eq.(10) for different values of C . We see that walls are smeared by the expansion as C approaches 2, whereas bigger C corresponds to thin wall. It is also noticeable that transition region is always at the de Sitter horizon.

From our simulations we see that the threshold for C is the same as in the case of planar walls.

We should note that de Sitter background is the only possibility to form domain walls with constant tension via Gauss-Bonnet term. If considered scenario takes place during cosmological inflation, then they would disappear during subsequent cosmological evolution because of spontaneous symmetry restoration induced, again, by Gauss-Bonnet term.

Let us consider Gauss-Bonnet term alone in FLRW background:

$$R_{GB}^2 = 24H^2(\dot{H} + H^2). \quad (12)$$

It is clear that during cosmological inflation $R_{GB}^2 = 24H^4$, which is a positive constant. However, it changes its sign as soon as $\ddot{a} = 0$, which would take place at some moment after inflation ends. For that reason, domain walls induced by Gauss-Bonnet symmetry breaking during cosmological inflation would disappear because of subsequent spontaneous Z_2 -symmetry restoration.

3.1. Loop corrections

For the EGB model defined in (1), and in the quasi-de Sitter regime where $H \simeq \text{const}$, the dynamics relevant for domain wall

formation is encoded in an effective single field description for ϕ with a Gauss-Bonnet induced mass shift. In what follows we include the leading quantum effects in this sector by working with the one-loop effective potential in the Coleman-Weinberg (CW) approximation, evaluated in the slowly varying de Sitter background. This captures the dominant radiative corrections to the scalar self-interactions and to the GB-induced effective mass, while keeping the analysis analytically tractable within the EGB framework.

At tree level the scalar sector is described by

$$V(\phi) = \frac{1}{2}m^2\phi^2 + \frac{1}{4}\lambda\phi^4 + \frac{3}{2}\alpha H^4\phi^2, \quad (13)$$

where the last term originates from the Gauss-Bonnet coupling. The GB interaction therefore induces an effective positive mass shift $\Delta m_{GB}^2 = \frac{3}{2}\alpha H^4$ for ϕ .

Quantum fluctuations generate radiative corrections which can be systematically included via the one-loop Coleman-Weinberg potential Coleman and Weinberg (1973),

$$\Delta V_1(\phi) = \frac{M^4(\phi)}{64\pi^2} \left[\ln \left(\frac{M^2(\phi)}{\mu^2} \right) - \frac{3}{2} \right], \quad (14)$$

with the field-dependent mass

$$M^2(\phi) = m^2 + 3\lambda\phi^2 + 3\alpha H^4. \quad (15)$$

The renormalization scale μ is chosen to minimize large logarithms, typically $\mu \sim \max\{|V''(\phi)|^{1/2}, H\}$, and the couplings (m^2, λ, α) are understood as running with μ Sher (1989); Lyth and Stewart (1992); Herranen et al. (2014); Markkanen and Tranberg (2019). In regions of field space where $M^2(\phi)$ becomes negative the one-loop expression formally develops an imaginary part signaling an instability. Following standard practice, and in order to avoid spurious complex contributions in our perturbative treatment, we consider $\ln M^2(\phi) \rightarrow \ln |M^2(\phi)|$ Weinberg and Wu (1987); Weinberg (2005); Parker and Toms (1985), keeping in mind that this choice effectively encodes the onset of spinodal dynamics which would require a real time analysis for a fully self-consistent description.

The one-loop effective potential is then

$$V_{\text{eff}}(\phi) = V(\phi) + \Delta V_1(\phi). \quad (16)$$

Variation of the effective action yields the corrected field equation,

$$\begin{aligned} \ddot{\phi} + 3H\dot{\phi} - e^{-2Ht} \left(\phi_{rr} + \frac{2}{r}\phi_r \right) + \phi \left(m^2 + \lambda\phi^2 + 3\alpha H^4 \right) \\ + \frac{3\lambda\phi}{8\pi^2} M^2(\phi) \left[\ln \left(\frac{M^2(\phi)}{\mu^2} \right) - 1 \right] = 0. \end{aligned} \quad (17)$$

We again introduce the similarity variable and rescaling (8)

$$u \equiv Hre^{Ht}, \quad \phi(u) = \eta f(u), \quad (18)$$

which reduces the problem to an ODE for $f(u)$:

$$H^2 \left[(u^2 - 1)f'' + \left(4u - \frac{2}{u}\right)f' \right] + m^2 f + \lambda \eta^2 f^3 + 3\alpha H^4 f + \frac{3\lambda f}{8\pi^2} \mathcal{M}^2(f) \left[\ln \left(\frac{\mathcal{M}^2(f)}{\mu^2} \right) - 1 \right] = 0, \quad (19)$$

with

$$\mathcal{M}^2(f) \equiv m^2 + 3\lambda \eta^2 f^2 + 3\alpha H^4. \quad (20)$$

Choosing the same normalization

$$\eta^2 = -\frac{3\alpha H^4 + m^2}{\lambda}, \quad (21)$$

and defining $\mu_0^2 \equiv m^2 + 3\alpha H^4$, we have $\lambda \eta^2 = -\mu_0^2$ and

$$\mathcal{M}^2(f) = \mu_0^2 (1 - 3f^2). \quad (22)$$

Therefore, our ODE becomes

$$(u^2 - 1)f'' + \left(4u - \frac{2}{u}\right)f' + \frac{|\mu_0^2|}{H^2} (f^3 - f) + \frac{3\lambda |\mu_0^2|}{8\pi^2 H^2} f(3f^2 - 1) \left[\ln \left(\frac{|\mu_0^2|(3f^2 - 1)}{\mu^2} \right) - 1 \right] = 0. \quad (23)$$

We can rewrite it in the similar way as (10)

$$(1 - u^2)f'' - \left(4u - \frac{2}{u}\right)f' = C f(f^2 - 1) + \frac{3\lambda C}{8\pi^2} f(3f^2 - 1) \left[\ln \left(C(3f^2 - 1) \right) - 1 \right], \quad (24)$$

where we introduced the dimensionless parameter

$$C \equiv \frac{|\mu_0^2|}{H^2}, \quad \mu \sim H, \quad \ln(M^2) \rightarrow \ln(|M^2|). \quad (25)$$

The GB term shifts the effective mass and together with Hubble friction create effect against the quartic self-interaction. Equation (24) therefore describes a “thick-wall” profile sourced by a cubic–quintic nonlinearity and a logarithmic radiative force. The parameter $C = |\mu_0^2|/H^2$ controls the wall thickness and the relative weight of mass versus friction: larger C typically sharpens the transition. The CW contribution modifies the profile slightly and can either sharpen or smooth the wall depending on λ and the local sign of $3f^2 - 1$. For the numerical solution we impose regularity at the origin, $f'(u \rightarrow 0) = 0$, and approach to a vacuum at large u . A fully self-consistent extension could incorporate slow time-dependence of $H(t)$ and RG-improved couplings along the profile, but the quasi-de Sitter and fixed- μ approximations adopted here capture the leading corrections and are standard in loop-corrected scalar dynamics in curved space-time Lyth and Stewart (1992); Guo and Schwarz (2010a); Kanti et al. (2015a); Herranen et al. (2014); Weinberg (2005); Parker and Toms (1985); Markkanen and Tranberg (2019); Figueroa et al. (2023); Weinberg and Wu (1987). The resulting numerical solutions with one-loop corrections are shown in Fig. 2b.

3.2. Constraints on parameters from inflation

In this section we derive constraint on λ . Note that this constraint occurs when the Z_2 symmetry is broken during cosmological inflation.

Let us estimate the energy density of the inflaton field ψ as follows:

$$\rho_{\text{inf}} = \frac{1}{2}\dot{\psi}^2 + V_{\text{inf}} \approx V_{\text{inf}} \sim H^2 M_{\text{Pl}}^2. \quad (26)$$

Planck data Planck Collaboration and Akrami, Y. (2020) provide constraint on Hubble parameter during cosmological inflation $H < 10^{14}$ GeV, so, taking $H \sim 10^{13}$ GeV, we got

$$\rho_{\text{inf}} \sim 10^{64} \text{ GeV}^4; E_{\text{inf}} = \rho_{\text{inf}} V_{\text{hor}} \sim M_{\text{Pl}}^2 H^{-1} \sim 10^{25} \text{ GeV}. \quad (27)$$

Let us now estimate mass of the wall and its energy density. In flat space-time we got corresponding characteristic width as follows:

$$\delta_0 = \sqrt{2}/\sqrt{\lambda}\eta = \sqrt{2}/\sqrt{-(3\alpha H^4 + m^2)}. \quad (28)$$

Surface energy density then is given by

$$\sigma = \frac{4}{3\sqrt{2}}\eta^3 \sqrt{\lambda} = \frac{4}{3\sqrt{2}} \frac{(-\alpha H^4 - m^2)^{3/2}}{\lambda}. \quad (29)$$

Finally, for thin wall (assume $|\alpha|H^4 \sim 10H^2 \gg m^2$) we can estimate mass of the wall as follows:

$$M_{\text{wall}} \sim 4\pi H^{-2} \sigma \sim 10^3 \frac{H}{\lambda} \sim \frac{10^{16} \text{ GeV}}{\lambda}. \quad (30)$$

For energy density of the wall we got:

$$T_{\text{max}}^{00} \sim \frac{10^3 H^4}{\lambda} \sim \frac{10^{55} \text{ GeV}^4}{\lambda}. \quad (31)$$

Constraint comes from the following condition:

$$T_{\text{max}}^{00} \ll \rho_{\text{inf}} \rightarrow \lambda \geq 10^{-8}. \quad (32)$$

From Fig.2b we see that $\lambda = 10^{-5}$ provides a small correction to the tree-level solution presented in Fig.1 and there are still a few orders of magnitude in a threshold for λ .

4. Setting up lattice simulations

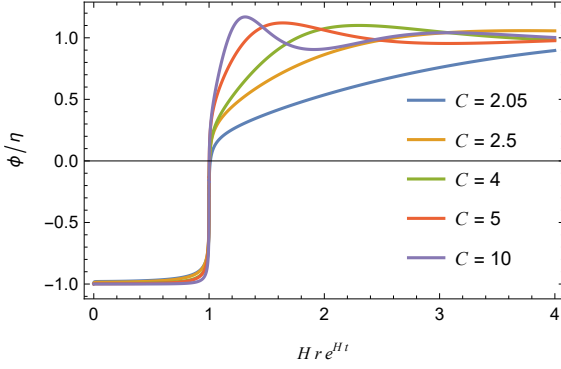
In this section we clarify our setup for lattice simulations using *CosmoLattice* package.

Following numerical analysis in Dankovsky et al. (2025b), we are going to study this package to calculate spectrum of gravitational waves (GW) emitted by domain walls.

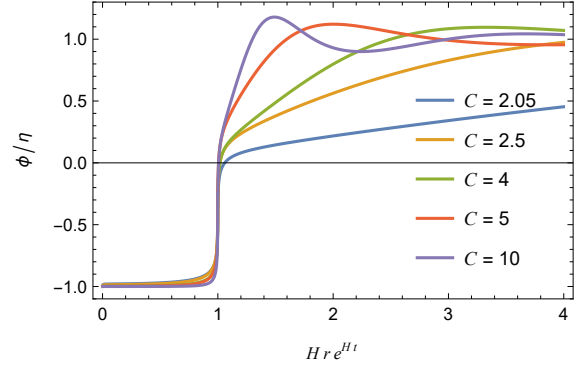
Here we start with some technical details about lattice:

$$\delta x = \frac{L}{N}, \quad k_{\text{IR}} = \frac{2\pi}{L} = \frac{2\pi}{N\delta x}, \quad k_{i,UV} = \frac{\pi}{\delta x}, \quad k_{\text{max}} = \sqrt{3}k_{i,UV}, \quad (33)$$

where δx is a grid step, k_{IR} is an infrared momentum cut-off corresponding to the grid step, which also defines physical size L of the lattice, $k_{i,UV}$ is ultraviolet momentum cut-off



(a) Domain wall's configuration without loop corrections. Same as Fig.1.



(b) Numerical solution of Eq. (24) for different values of $C = |\mu_0^2|/H^2$. Here $\lambda = 10^{-5}$. Increasing C generally narrows the wall, while the one-loop Coleman–Weinberg term induces a small, parameter-dependent shift of the profile.

Figure 2: Comparison of domain wall's static configurations with and without loop correction.

corresponding to one dimension of the grid and k_{max} is defined as maximal momentum, which is calculated as $k_{max} = \sqrt{k_{x,UV}^2 + k_{y,UV}^2 + k_{z,UV}^2}$.

Now let us delve into scalar field dynamics. *CosmoLattice* operates with dimensionless units as follows:

$$\phi \rightarrow \tilde{\phi} = \frac{\phi}{f_\star}, \quad dx^i \rightarrow d\tilde{x}^i = \omega_\star dx^i, \quad V \rightarrow \tilde{V} = \frac{V}{f_\star^2 \omega_\star^2}, \quad (34)$$

where f_\star and ω_\star are somehow defined through model's parameters. We would specify our values of f_\star and ω_\star below.

Following recommendations given in *CosmoLattice* manual Figueroa et al. (2023), we would simulate field's dynamics in conformal FLRW spacetime. This particular recommendation follows from field's potential. Namely, authors suggest to utilize conformal FLRW metric if scalar field's potential contains polynomial terms up to quartic, which is our case.

We utilize vacuum initial conditions with quantum fluctuations defined by power spectrum. Initial quantum vacuum fluctuations could be written as follows:

$$\begin{aligned} \langle \delta\phi^2 \rangle &= \int d \log k \Delta_{\delta\phi}(k), \quad \Delta_{\delta\phi}(k) = \frac{k^3}{2\pi^2} \mathcal{P}_{\delta\phi}(k), \quad \langle \delta\phi_k \delta\phi_{k'} \rangle \\ &= (2\pi)^3 \mathcal{P}_{\delta\phi}(k) \delta(\mathbf{k} - \mathbf{k}'), \end{aligned} \quad (35)$$

where $\langle \dots \rangle$ represents an average value and the power spectrum is given as follows:

$$\mathcal{P}_{\delta\phi}(k) = \frac{1}{2a^2 \omega_{k,\phi}}, \quad \omega_{k,\phi} = \sqrt{k^2 + a^2 m_\phi^2}, \quad m_\phi^2 = \left. \frac{\partial^2 V}{\partial \phi^2} \right|_{\phi=\phi_*}, \quad (36)$$

where V contains Gauss-Bonnet term. In this expression, $\omega_{k,\phi}$ is the frequency of the mode, and m_ϕ^2 is the effective mass of the scalar field, evaluated by the initial homogeneous amplitude ϕ_* of the given scalar field.

Initial fluctuations are governed by k_{cut} , which represent the cut-off in the spectrum of fluctuations. This cut-off is defined by user.

Now we specify the model to simulate scalar field's dynamics. Let us consider the following Lagrangian:

$$\mathcal{L} = \sqrt{-g} \left(\frac{R}{2} + g^{\mu\nu} \partial_\mu \phi \partial_\nu \phi - V(\phi) - \frac{1}{8} \xi(\phi) R_{GB}^2 \right), \quad (37)$$

where V and ξ are defined in the same way as in the previous section:

$$\xi(\phi) = \frac{1}{2} \alpha \phi^2, \quad V(\phi) = \frac{1}{2} m^2 \phi^2 + \frac{1}{4} \lambda \phi^4. \quad (38)$$

In conformal FLRW given by line element

$$ds^2 = a^2(\tau)(d\tau^2 - d\mathbf{x}^2), \quad (39)$$

GB-term is found to be equal to:

$$R_{GB}^2 = \frac{24(a a'^2 a'' - a'^4)}{a^8}, \quad (40)$$

where prime represents derivative with respect to conformal time τ . We can now write equation of motion for the scalar field in conformal FLRW:

$$\frac{1}{a^2} \phi'' + 2 \frac{a'}{a^3} \phi' - \frac{1}{a^2} \partial_i^2 \phi + V_\phi + \frac{1}{8} \xi_\phi R_{GB}^2 = 0 \quad (41)$$

and alternatively:

$$\phi'' + 2 \frac{a'}{a} \phi' - \partial_i^2 \phi + a^2 \left(V_\phi + \frac{1}{8} \xi_\phi R_{GB}^2 \right) = 0. \quad (42)$$

We are interested in radiation dominated (RD) epoch, then the scale factor is as follows:

$$a(\tau) = (\tau/\tau_0), \quad (43)$$

where τ_0 refers to the start of field's motion (or start of the simulation).

In the process of simulations we have found that potential energy of the scalar field ϕ becomes negligible compared to $\dot{\phi}^2$

and $(\nabla\phi)^2$ after just one Hubble time. It is easy to understand, because in our model symmetry is initially broken by GB term which decreases rapidly with time. We remind that in conformal FLRW in radiational background it is as follows:

$$R_{GB}^2 = \frac{24(aa'^2a'' - a'^4)}{a^8} \propto \tau^{-8}. \quad (44)$$

Now let us put Eq.(38) in Eq.(42), then we obtain

$$\phi'' + 2\frac{a'}{a}\phi' - \partial_i^2\phi + \lambda\phi a^2\left(\phi^2 + \frac{m^2}{\lambda} - 3\frac{\alpha}{\lambda\tau_0^4(\tau/\tau_0)^8}\right) = 0. \quad (45)$$

We can now introduce vacuum expectation value (VEV):

$$\eta^2(\tau) = \frac{3\alpha}{\lambda\tau_0^4(\tau/\tau_0)^8} - \frac{m^2}{\lambda}. \quad (46)$$

Given with definition of VEV, we can now specify f_\star and ω_\star . In our model we set them to be equal to:

$$f_\star = \eta(\tau_i), \omega_\star = \sqrt{\lambda}f_\star. \quad (47)$$

Equation (42) could be simplified dramatically. Let us substitute

$$\phi = \frac{s}{a}, \quad (48)$$

then we obtain:

$$s'' - \partial_i^2 s + \lambda s(s^2 - a^2\eta^2) - \frac{a''}{a}s = 0. \quad (49)$$

During RD epoch we have $a'' = 0$, so we have very simple EoM:

$$s'' - \partial_i^2 s + \lambda s(s^2 - a^2\eta^2) = 0. \quad (50)$$

Equation (50) is basically equation of motion in Minkowski space. Let us introduce $\eta' = a\eta$, then in terms of field s we have the following time dependence of wall's tension on time:

$$\sigma(\tau) = \frac{2\sqrt{2}\lambda\eta'^3}{3} = \frac{2\sqrt{2}\lambda}{3}\left(\frac{3\alpha}{\lambda\tau_0^4(\tau/\tau_0)^6} - \frac{m^2(\tau/\tau_0)^2}{\lambda}\right)^{3/2}. \quad (51)$$

One can easily found the time when Z_2 symmetry is restored, if it is initially broken ($\eta(\tau_0) > 0$):

$$\sigma(\tau_{end}) = 0 \rightarrow \tau_{end} = \sqrt{\tau_0}\left(\frac{3\alpha}{m^2}\right)^{1/8}. \quad (52)$$

Given with such time dependence of VEV and wall's tension, it is now clear that walls would melt rapidly within this particular model introduced by Lagrangian (37).

In the following sections we would study possible observable consequences of scalar field's motion coupled with Gauss-Bonnet term. Namely we would study emission of gravitational waves and possibility of black hole formation.

We should also note that *CosmoLattice* by default define fraction of energy density of gravitational waves as $\Omega_{GW} = \frac{\tilde{\rho}_{GW}}{\tilde{\rho}_{tot}} \neq$

$\frac{\tilde{\rho}_{GW}}{\tilde{\rho}_c}$, where ρ_{tot} refers to the energy density of matter fields which are programmed by user, so it does not take into account critical density of the Universe. For that reason output should be multiplied by corresponding factor to restore common definition. In program units critical density would be as follows:

$$\tilde{\rho}_c(\tau) = \frac{\rho_c(\tau)}{f_\star^2\omega_\star^2} = \frac{3\lambda M_{pl}^2}{8\pi H_0^2 a^4(\tau)} \quad (53)$$

and standart definition is then restored as follows:

$$\Omega_{GW} = \frac{\tilde{\rho}_{GW}}{\tilde{\rho}_{tot}} \cdot \frac{\tilde{\rho}_{tot}}{\tilde{\rho}_c}. \quad (54)$$

Throughout our paper we would operate with standart definition of fraction of energy density.

We would like to finalize this section by clarifying exact values, which we utilize in our simulations. We set $N = 256$, $k_{IR} = 0.1$ and $k_{cut} = 4$.

5. GWs emitted during RD epoch

In this next section we present our results of gravitational wave's spectra assuming background is radiation dominated. We utilize vacuum initial conditions with initial fluctuations defined in the previous section.

For now, let us specify the value of α , which is coupling constant between scalar field and Gauss-Bonnet term. Classical motion of the field starts when its effective mass is of order of Hubble parameter, for that reason we choose

$$\alpha = \frac{1}{3H_0^2}, \quad (55)$$

where H_0 is the Hubble parameter at the start of the motion (simulations). We should note that in radiational background we need positive value of coupling constant α to have initially broken Z_2 symmetry. We would like to remind the reader that we assume $m^2 > 0$ and we set this term to be small so that it is negligible compared with Gauss-Bonnet coupling term at the start of the motion in order to have a possibility to form walls.

Given with Eq.(55), we can now represent f_\star and ω_\star via Hubble parameter at the start of the motion H_0 and λ :

$$\eta(\tau_0) = \frac{H_0}{\sqrt{\lambda}}, \omega_\star = H_0. \quad (56)$$

At this point our model has three free parameters: H_0 , m and λ .

Now we study the impact of model's parameters on gravitational wave's spectra.

Let us study impact of m . Presence of non-zero positive mass would eventually lead to spontaneous restoration of Z_2 symmetry. We can now calculate a certain moment of time τ_{end} at which symmetry is restored. Let us set $m = \beta H_0$, then we obtain:

$$\tau_{end} = \sqrt{\tau_0}\left(\frac{3\alpha}{m^2}\right)^{1/8} = \frac{1}{H_0\beta^{1/4}}. \quad (57)$$

Let us assume $\beta = 10^{-3}$, then

$$\tau_{end} \approx 5.62\tau_i. \quad (58)$$

Given with that value above we set the duration of simulations to be $\tau_f = 10\tau_0$. We demonstrate GW spectra for $H_0 = 10^{-5}\text{GeV}$ and $\lambda = 10^{-8}$. Please, see Fig.3 and Fig.4.

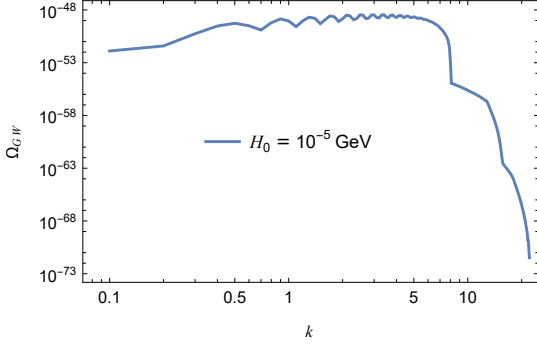


Figure 3: Spectrum of GWs during RD stage. Duration of simulations $\tau_f = 10\tau_i$ and $m = 10^{-3}H_0$.

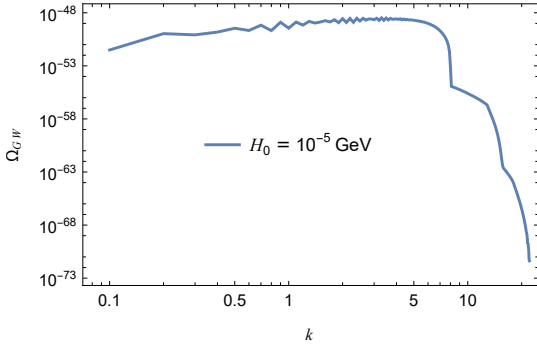


Figure 4: Spectrum of GWs during RD stage. Time of simulations $\tau_f = 10\tau_i$ and $m = 0$.

From Fig.3 and Fig.4 one can notice a difference in between plots in the area of small momentum, but this area is far from the peak of the spectrum, thus impact of mass could be observed only if waves corresponding to these momenta could be detected. One may see the value of Ω_{GW} is extremely low here and cannot be detected by modern detectors. this result seems natural because Gauss-Bonnet term decreases rapidly with time and mass term in the model is set to be small by assumption. Here we conclude that the parameter m is irrelevant in terms of the detectability of the spectrum.

Then we progress by fixing value of $\lambda = 10^{-8}$ and study impact of initial Hubble parameter. Here we also set $m = 0$ to simplify simulations. We demonstrate our findings in Fig.5. Gravitational waves are mostly emitted during the start of the field's motion. By *CosmoLattice* we find that GW energy density starts to behave as a radiational background after just a few Hubble times after the start of the simulations.

From Fig.5 we conclude

$$\Omega_{GW}(H) = (H/H_0)^4 \Omega_{GW}(H_0). \quad (59)$$

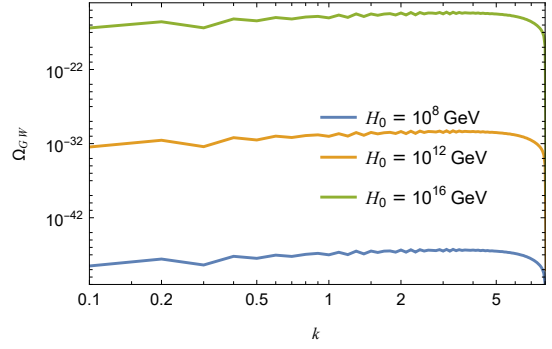


Figure 5: Spectrum of GWs during RD stage. Here we compare spectra obtained with different initial Hubble parameters. One can easily see strong dependence on its value. Although even for unrealistically high values of H_0 does not produce detectable spectrum.

Finally, we study impact of λ . We present our in Fig.6.

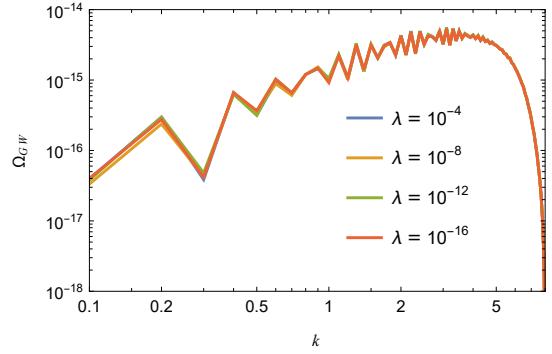


Figure 6: Spectrum of GWs during RD stage. One can see Ω_{GW} is independent of λ . Here we set $H_0 = 10^{16}\text{GeV}$ and $m = 0$.

From the plot in Fig.6 we can see that dependence on λ of the spectrum is basically negligible.

At this point, via *Comolattice* simulations we have found that GWs spectra effectively depends only on initial Hubble parameter H_0 in our model.

Now, let us present spectra calculated at modern times as a function of frequency. Here we set the duration of the simulations $\tau_f = 20\tau_0$.

Transformation from program variables to frequency is as follows:

$$F = \frac{H_0 k}{2\pi(z_0 + 1)}, \quad (60)$$

which means that the frequency depends on the initial Hubble parameter, since $k[\text{GeV}] = \omega_\star k = H_0 k$. In the expression above z_0 is the redshift corresponding to the start of field's motion or simulations.

We now utilize the Hubble law to calculate redshift:

$$H(z)^2 = H_{modern}^2 (\Omega_r(1+z)^4 + \Omega_m(1+z)^3 + \Omega_\Lambda), \quad H_{modern} \sim 10^{-42} \text{ GeV}. \quad (61)$$

One can approximately estimate the redshift as:

$$z_0 \approx \left(\frac{H(z_0)^2}{\Omega_r H_{\text{modern}}^2} \right)^{1/4}, \quad (62)$$

since we consider RD epoch. By considering different initial Hubble parameters, we are considering different redshifts.

Finally, frequency corresponding to modern Universe is calculated as follows:

$$F = \frac{(H_0 H_{\text{modern}})^{1/2} \Omega_r^{1/4}}{2\pi} k. \quad (63)$$

We are now ready to present GW spectra corresponding to modern times. Please, see Fig.7 and Fig.8.

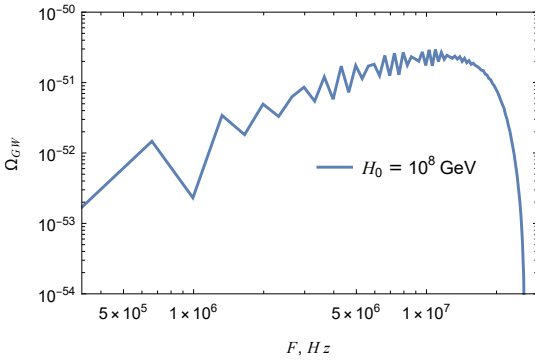


Figure 7: GWs spectrum as a function of frequency, which corresponds to modern Universe. Here Ω_{GW} is normalized by modern critical density, taking into account time dependence of GW's energy density.

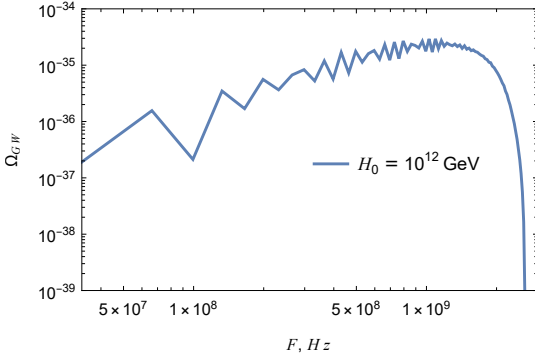


Figure 8: GWs spectrum as a function of frequency, which corresponds to modern Universe. Here Ω_{GW} is normalized by modern critical density, taking into account time dependence of GW's energy density.

Let us now estimate strain corresponding to the spectrum in Fig.8. We start with definition:

$$\Omega_{GW} = \frac{2\pi^2}{3H_{\text{modern}}^2} f^3 S_h(f) \rightarrow \sqrt{S_h(f)} = \sqrt{\frac{3\Omega_{GW} H_{\text{modern}}^2}{2\pi^2 f^3}}. \quad (64)$$

Taking peak frequency and maximum value of Ω_{GW} in Fig. 8, estimation of strain is as follows:

$$\sqrt{S_h} \sim 10^{-48} \sqrt{\text{Hz}}^{-1}. \quad (65)$$

Let us now discuss the possibility of detection of such GWs. From paper Collaboration et al. (2025) it is clear that modern facilities are incapable of detecting such weak waves. Though there is at least a chance that these waves could be detected by future detectors Cai et al. (2025). In aggressive optical Raman schemes there could be achieved sensitivity up to

$$\sqrt{S_{h,\text{min}}} \sim 10^{-37} \sqrt{\text{Hz}}^{-1} \quad (66)$$

in THz range, which is not applicable to our findings.

Recent researches have demonstrated that in the terahertz range, the graviton-to-photon conversion process can be resonantly amplified by cosmological magnetic fields Addazi et al. (2024c, 2025). While this makes the detection of very high-frequency gravitational waves via radio astronomy theoretically possible, the signal strength for our specific case remains too weak for any radio-astronomy instruments planned for the foreseeable future.

Thus, in the future, our model could be found true or constrained. Namely, since we expressed everything in terms of the initial Hubble parameter at the start of the scalar field motion, possible constraints would restrict the value of the coupling constant α .

6. Primordial Black Hole formation: a no-go argument

In this section we study the possibility of PBH formation within considered model.

Let us start with clarification of wall's width dependence on the scale factor:

$$\delta_{\text{wall}}(\tau) = \frac{\sqrt{2}}{\sqrt{\lambda}\eta'(\tau)} = \frac{\sqrt{2}}{\sqrt{\frac{3\alpha H_0^4}{a^6} - m^2 a^2}} > \frac{a^3 \sqrt{2}}{H_0^2 \sqrt{3\alpha}} = \frac{a^3 \sqrt{2}}{H_0} = \frac{a^3 \sqrt{2}}{\omega_\star}. \quad (67)$$

From the expression above, we conclude that walls in our model are smeared by the expansion, unlike in the case of walls with constant surface energy density.

We recall tension given by Eq.(51):

$$\sigma(\tau) = \frac{2\sqrt{2}\lambda\eta^3}{3} = \frac{2\sqrt{2}\lambda}{3} \left(\frac{3\alpha}{\lambda\tau_0^4(\tau/\tau_0)^6} - \frac{m^2(\tau/\tau_0)^2}{\lambda} \right)^{3/2}. \quad (68)$$

One can estimate the mass of the domain wall m_w as follows:

$$m_w(\tau) = 4\pi\sigma(\tau)u_w^2, \quad (69)$$

where u_w is the radius of the wall. This leads to the following relation between the wall's gravitational radius and the wall's radius:

$$u_g(\tau) = 2Gm(\tau) = 8\pi G\sigma(\tau)u_w^2(\tau). \quad (70)$$

Now let us compare u_w and u_g :

$$\frac{u_g}{u_w} = 8\pi G\sigma(\tau)u_w(\tau). \quad (71)$$

To form a black hole it is required

$$\frac{u_g}{u_w} > 1 \rightarrow u_w(\tau) > \frac{3\lambda}{16\pi G \sqrt{2} \left(\frac{3\alpha}{\tau_0^4 a^6(\tau)} - m^2 a^2(\tau) \right)^{3/2}}. \quad (72)$$

Expression Eq.(72) shows the condition under which it is possible to form a PBH. Let us put $m = 0$ to weaken that condition:

$$u_w(\tau) > \frac{3\lambda}{16\sqrt{2}\pi G H_0^3} a^9(\tau). \quad (73)$$

Expression above indicates that, in order to make PBH formation possible, it is demanded a walls expansion rate which is faster than a^9 . Such a possibility is forbidden since it demands an impossible superluminal expansion of domain walls. Walls are considered as being at rest relative to the Hubble expansion, implying their radius evolves as the scale factor with time $u_w = u_0 a$, where u_0 is initial radius of the wall.

Now let us compare gravitational radius to wall's width:

$$\frac{u_g}{\delta} = \frac{8\pi G \sigma u_w^2}{\delta} = \frac{16\pi G u_0^2 H_0^4}{3\lambda a^{10}} \propto \frac{1}{a^{10}}, \quad (74)$$

which demonstrates even stronger condition compared to wall's radius.

From the expressions above we conclude that it is impossible to form black holes within this model (from the collapse of domain walls). Conditions given by (72) and (74) cannot be satisfied in reality.

7. Discussions and Conclusions

In this paper, we analyzed possible observable effects arising from the spontaneous Z_2 symmetry breaking or restoration that is catalyzed by the Gauss-Bonnet term. Our investigation is built upon a specific formulation of the scalar-Gauss-Bonnet coupling constant α .

Our investigation commenced with an analysis of domain wall formation in a de Sitter (inflationary) background. Throughout this epoch, the Gauss-Bonnet term remains nearly constant. Our analysis demonstrated the existence of static domain wall solutions characterized by a constant proper width. The threshold for parameter C in our model was found to be the same as in previous works by *Dolgov & Vilenkin* Dolgov et al. (2016, 2018); Basu and Vilenkin (1994). Finally, we found that in the spherically symmetric case, the domain wall's transitional region is located precisely at the de Sitter horizon.

Subsequently, we examined the scalar field evolution within a radiation-dominated Universe. Here, the Gauss-Bonnet term diminishes rapidly, which provides a specific mechanism for wall's melting. The melting process was found to be very rapid – much faster than in the cases considered by *Dankovsky, Ramazanov, Babichev et al* Dankovsky et al. (2024, 2025b,a). While prior work assumes the VEV scales inversely with the scale factor, our model ties its evolution to the Gauss-Bonnet term, resulting in accelerated decay. Using the *Cosmo-Lattice* package, we analyze this scenario to assess GWs emission from the melting walls and the associated PBH production.

Our results showed a strong dependence of the GW spectrum on the initial Hubble parameter when the scalar field evolution begins. Unfortunately, the predicted GW spectra are likely to be undetectable even by next-generation observatories. However, future detectors could potentially place mild constraints on the model parameters. The analysis further reveals that, due to the rapid melting process, the wall's radius and width must expand with impossible superluminal velocity to eventually become gravitationally self-enclosed. Consequently, PBH formation is ruled out in this scenario.

To summarize, our model predicts signals below foreseeable detection thresholds. This result serves as a no-go argument for GB theories of this class, and is robust for any regular coupling function $\xi(\phi)$.

In the present work, we have not accounted for the potential dynamics of domain-wall melting and decay within the early-universe plasma. Recent numerical studies of gravitational-wave generation from first-order cosmological phase transitions FOCPT indicate that the dominant signal often originates not from the direct collision of bubble walls, but from the subsequent acoustic (sound-wave) oscillations and magnetohydrodynamic (MHD) turbulence induced in the plasma by the walls' expansion Hindmarsh et al. (2014) – this case seems also favored as an explanation of NANOGrav excess from FOCPTs Addazi et al. (2024b) (see also Addazi et al. (2018, 2021). By analogy, a rapid melting or “despairing” of a domain-wall network could likewise transfer substantial energy into the surrounding plasma, thereby exciting sound waves and MHD turbulence capable of sourcing a stochastic gravitational-wave background. The characteristics of such a signal would depend crucially on the network's scaling properties at decay, the timescale of melting relative to the Hubble time, and the efficiency with which wall energy is converted into bulk fluid motion. A reliable prediction requires dedicated numerical simulations of a coupled scalar-field and relativistic-fluid system, capturing the decay of the network and the resulting plasma dynamics. Future work should therefore investigate this possibility through large-scale simulations, analogous to those performed for phase transitions, in order to determine whether plasma-mediated effects could dominate the gravitational-wave signature—or even constitute the primary observable signal—of a transient domain-wall network in the Early Universe.

Acknowledgments

We are grateful to V. Nikulin and I. Dankovsky for fruitful discussions and interest in our work. The work of M. Kr. was performed in Southern Federal University with financial support of grant of Russian Science Foundation № 25-07-IF. AA work is supported by the National Science Foundation of China (NSFC) through the grant No. 12350410358; the Talent Scientific Research Program of College of Physics, Sichuan University, Grant No. 1082204112427; the Fostering Program in Disciplines Possessing Novel Features for Natural Science of Sichuan University, Grant No.2020SCUNL209 and 1000 Talent program of Sichuan province 2021.

References

- Abbott, B.P., et al. (LIGO Scientific, Virgo), 2016. Observation of Gravitational Waves from a Binary Black Hole Merger. *Phys. Rev. Lett.* 116, 061102. doi:10.1103/PhysRevLett.116.061102, arXiv:1602.03837.
- Abbott, B.P., et al. (LIGO Scientific, Virgo), 2017. GW170817: Observation of Gravitational Waves from a Binary Neutron Star Inspiral. *Phys. Rev. Lett.* 119, 161101. doi:10.1103/PhysRevLett.119.161101, arXiv:1710.05832.
- Addazi, A., Aldabergenov, Y., Cai, Y., 2024a. Sound speed resonance of gravitational waves in Gauss-Bonnet-coupled inflation. *Phys. Rev. D* 110, 123530. doi:10.1103/PhysRevD.110.123530, arXiv:2408.05091.
- Addazi, A., Cai, Y.F., Gan, Q., Marciano, A., Zeng, K., 2021. NANOGrav results and dark first order phase transitions. *Sci. China Phys. Mech. Astron.* 64, 290411. doi:10.1007/s11433-021-1724-6, arXiv:2009.10327.
- Addazi, A., Cai, Y.F., Marciano, A., 2018. Testing Dark Matter Models with Radio Telescopes in light of Gravitational Wave Astronomy. *Phys. Lett. B* 782, 732–736. doi:10.1016/j.physletb.2018.06.015, arXiv:1712.03798.
- Addazi, A., Cai, Y.F., Marciano, A., Visinelli, L., 2024b. Have pulsar timing array methods detected a cosmological phase transition? *Phys. Rev. D* 109, 015028. doi:10.1103/PhysRevD.109.015028, arXiv:2306.17205.
- Addazi, A., Capozziello, S., Gan, Q., 2024c. Resonant graviton-photon transitions with cosmological stochastic magnetic field. *Phys. Lett. B* 851, 138574. doi:10.1016/j.physletb.2024.138574.
- Addazi, A., Capozziello, S., Gan, Q., 2025. Resonant graviton-photon conversion with stochastic magnetic field in the expanding universe. *Phys. Dark Univ.* 48, 101844. doi:10.1016/j.dark.2025.101844, arXiv:2401.15965.
- Aldabergenov, Y., Berkimbayev, D., 2025. Gauss-bonnet-induced symmetry breaking/restoration during inflation. *Universe* 11, 98. URL: <http://dx.doi.org/10.3390/universe11030098>, doi:10.3390/universe11030098.
- Babichev, E., Gorbunov, D., Ramazanov, S., Samanta, R., Vikman, A., 2023. NANOGrav spectral index $\gamma=3$ from melting domain walls. *Phys. Rev. D* 108, 123529. doi:10.1103/PhysRevD.108.123529, arXiv:2307.04582.
- Basu, R., Guth, A.H., Vilenkin, A., 1991. Quantum creation of topological defects during inflation. *Phys. Rev. D* 44, 340–351. URL: <https://link.aps.org/doi/10.1103/PhysRevD.44.340>, doi:10.1103/PhysRevD.44.340.
- Basu, R., Vilenkin, A., 1994. Evolution of topological defects during inflation. *Physical Review D* 50, 7150–7153. URL: <http://dx.doi.org/10.1103/PhysRevD.50.7150>, doi:10.1103/physrevd.50.7150.
- Cai, Y.F., Visinelli, L., Yan, S.F., 2025. Atomic quantum sensors for high-frequency gravitational wave searches. URL: <https://arxiv.org/abs/2510.15031>, arXiv:2510.15031.
- Cartier, C., Hwang, J.c., Copeland, E.J., 2001. Evolution of cosmological perturbations in nonsingular string cosmologies. *Phys. Rev. D* 64, 103504. doi:10.1103/PhysRevD.64.103504, arXiv:astro-ph/0106197.
- Clough, K., Helfer, T., Witek, H., Berti, E., 2022. Ghost instabilities in self-interacting vector fields: The problem with proca fields. *Physical Review Letters* 129. URL: <http://dx.doi.org/10.1103/PhysRevLett.129.151102>, doi:10.1103/physrevlett.129.151102.
- Coleman, S., Weinberg, E., 1973. Radiative corrections as the origin of spontaneous symmetry breaking. *Phys. Rev. D* 7, 1888–1910. URL: <https://link.aps.org/doi/10.1103/PhysRevD.7.1888>, doi:10.1103/PhysRevD.7.1888.
- Collaboration, T.L.S., the Virgo Collaboration, the KAGRA Collaboration, 2025. Upper limits on the isotropic gravitational-wave background from the first part of ligo, virgo, and kagra’s fourth observing run. URL: <https://arxiv.org/abs/2508.20721>, arXiv:2508.20721.
- Dadhich, N., 2005. On the Gauss-Bonnet gravity, in: 12th Regional Conference on Mathematical Physics, pp. 331–340. arXiv:hep-th/0509126.
- Dankovsky, I., Babichev, E., Gorbunov, D., Ramazanov, S., Vikman, A., 2024. Revisiting evolution of domain walls and their gravitational radiation with cosmolattice. *Journal of Cosmology and Astroparticle Physics* 2024, 047. URL: <http://dx.doi.org/10.1088/1475-7516/2024/09/047>, doi:10.1088/1475-7516/2024/09/047.
- Dankovsky, I., Ramazanov, S., Babichev, E., Gorbunov, D., Vikman, A., 2025a. Cosmic domain walls on a lattice: illusive effects of initial conditions. URL: <https://arxiv.org/abs/2509.25367>, arXiv:2509.25367.
- Dankovsky, I., Ramazanov, S., Babichev, E., Gorbunov, D., Vikman, A., 2025b. Numerical analysis of melting domain walls and their gravitational waves. *Journal of Cosmology and Astroparticle Physics* 2025, 064. URL: <https://dx.doi.org/10.1088/1475-7516/2025/02/064>, doi:10.1088/1475-7516/2025/02/064.
- Dolgov, A., Godunov, S., Rudenko, A., 2016. Evolution of thick domain walls in de sitter universe. *Journal of Cosmology and Astroparticle Physics* 2016, 026–026. URL: <http://dx.doi.org/10.1088/1475-7516/2016/10/026>, doi:10.1088/1475-7516/2016/10/026.
- Dolgov, A.D., Godunov, S.I., Rudenko, A.S., 2018. Evolution of thick domain walls in inflationary and $p = w\rho$ universe. *The European Physical Journal C* 78. URL: <http://dx.doi.org/10.1007/s10052-018-6000-0>, doi:10.1007/s10052-018-6000-0.

- doi.org/10.1140/epjc/s10052-018-6350-7, doi:10.1140/epjc/s10052-018-6350-7.
- Doneva, D.D., Yazadjiev, S.S., 2018. New gauss-bonnet black holes with curvature-induced scalarization in extended scalar-tensor theories. *Physical Review Letters* 120. URL: <http://dx.doi.org/10.1103/PhysRevLett.120.131103>, doi:10.1103/physrevlett.120.131103.
- Fernandes, P.G.S., Carrilho, P., Clifton, T., Mulryne, D.J., 2022. The 4d einstein-gauss-bonnet theory of gravity: a review. *Classical and Quantum Gravity* 39, 063001. URL: <http://dx.doi.org/10.1088/1361-6382/ac500a>, doi:10.1088/1361-6382/ac500a.
- Figueroa, D.G., Florio, A., Torrenti, F., Valkenburg, W., 2021. The art of simulating the early universe. part i. integration techniques and canonical cases. *Journal of Cosmology and Astroparticle Physics* 2021, 035. URL: <http://dx.doi.org/10.1088/1475-7516/2021/04/035>, doi:10.1088/1475-7516/2021/04/035.
- Figueroa, D.G., Florio, A., Torrenti, F., Valkenburg, W., 2023. Cosmolattice: A modern code for lattice simulations of scalar and gauge field dynamics in an expanding universe. *Computer Physics Communications* 283, 108586. URL: <http://dx.doi.org/10.1016/j.cpc.2022.108586>, doi:10.1016/j.cpc.2022.108586.
- Ghosh, S.G., Kumar, R., 2020. Generating black holes in 4d einstein-gauss-bonnet gravity. *Classical and Quantum Gravity* 37, 245008. URL: <https://doi.org/10.1088/1361-6382/abc134>, doi:10.1088/1361-6382/abc134.
- Gregory, R., 2011. Holographic superconductivity with gauss-bonnet gravity. *Journal of Physics: Conference Series* 283, 012016. URL: <https://doi.org/10.1088/1742-6596/283/1/012016>, doi:10.1088/1742-6596/283/1/012016.
- Guerrero, R., Rodriguez, R.O., Torrealba, R., Ortiz, R., 2006. De sitter and double irregular domain walls. *General Relativity and Gravitation* 38, 845–855. URL: <http://dx.doi.org/10.1007/s10714-006-0297-y>, doi:10.1007/s10714-006-0297-y.
- Guo, Z.K., Schwarz, D.J., 2009. Power spectra from an inflaton coupled to the Gauss-Bonnet term. *Phys. Rev. D* 80, 063523. doi:10.1103/PhysRevD.80.063523, arXiv:0907.0427.
- Guo, Z.K., Schwarz, D.J., 2010a. Slow-roll inflation with a gauss-bonnet correction. *Physical Review D* 81, 123520. URL: <http://dx.doi.org/10.1103/PhysRevD.81.123520>, doi:10.1103/PhysRevD.81.123520.
- Guo, Z.K., Schwarz, D.J., 2010b. Slow-roll inflation with a Gauss-Bonnet correction. *Phys. Rev. D* 81, 123520. doi:10.1103/PhysRevD.81.123520, arXiv:1001.1897.
- Herranen, M., Markkanen, T., Nurmi, S., Rajantie, A., 2014. Spacetime curvature and the higgs stability during inflation. *Physical Review Letters* 113, 211102. URL: <http://dx.doi.org/10.1103/PhysRevLett.113.211102>, doi:10.1103/PhysRevLett.113.211102.
- Himmetoglu, B., Contaldi, C.R., Peloso, M., 2009. Ghost instabilities of cosmological models with vector fields non-minimally coupled to the curvature. *Physical Review D* 80. URL: <http://dx.doi.org/10.1103/PhysRevD.80.123530>, doi:10.1103/physrevd.80.123530.
- Hindmarsh, M., Huber, S.J., Rummukainen, K., Weir, D.J., 2014. Gravitational waves from the sound of a first order phase transition. *Phys. Rev. Lett.* 112, 041301. doi:10.1103/PhysRevLett.112.041301, arXiv:1304.2433.
- Hwang, J.c., Noh, H., 2000. Conserved cosmological structures in the one loop superstring effective action. *Phys. Rev. D* 61, 043511. doi:10.1103/PhysRevD.61.043511, arXiv:astro-ph/9909480.
- Hwang, J.c., Noh, H., 2005. Classical evolution and quantum generation in generalized gravity theories including string corrections and tachyon: Unified analyses. *Phys. Rev. D* 71, 063536. doi:10.1103/PhysRevD.71.063536, arXiv:gr-qc/0412126.
- Jiang, P.X., Hu, J.W., Guo, Z.K., 2013. Inflation coupled to a Gauss-Bonnet term. *Phys. Rev. D* 88, 123508. doi:10.1103/PhysRevD.88.123508, arXiv:1310.5579.
- Kanti, P., Gannouji, R., Dadhich, N., 2015a. Gauss-bonnet inflation. *Physics Letters B* 734, 27–33. URL: <http://dx.doi.org/10.1016/j.physletb.2014.11.013>, doi:10.1016/j.physletb.2014.11.013.
- Kanti, P., Gannouji, R., Dadhich, N., 2015b. Gauss-Bonnet Inflation. *Phys. Rev. D* 92, 041302. doi:10.1103/PhysRevD.92.041302, arXiv:1503.01579.
- Kawaguchi, R., Tsujikawa, S., 2023. Primordial black holes from Higgs inflation with a Gauss-Bonnet coupling. *Phys. Rev. D* 107, 063508. doi:10.1103/PhysRevD.107.063508, arXiv:2211.13364.
- Kawai, S., Kim, J., 2019. Gauss-Bonnet Chern-Simons gravitational wave leptogenesis. *Phys. Lett. B* 789, 145–149. doi:10.1016/j.physletb.2018.12.019, arXiv:1702.07689.
- Kawai, S., Kim, J., 2021a. CMB from a Gauss-Bonnet-induced de Sitter fixed point. *Phys. Rev. D* 104, 043525. doi:10.1103/PhysRevD.104.043525, arXiv:2105.04386.
- Kawai, S., Kim, J., 2021b. Primordial black holes from Gauss-Bonnet-corrected single field inflation. *Phys. Rev. D* 104, 083545. doi:10.1103/PhysRevD.104.083545, arXiv:2108.01340.

- Kawai, S., Sakagami, M.a., Soda, J., 1998. Instability of one loop superstring cosmology. *Phys. Lett. B* 437, 284–290. doi:10.1016/S0370-2693(98)00925-3, arXiv:gr-qc/9802033.
- Kleihaus, B., Kunz, J., Radu, E., 2011. Rotating black holes in dilatonic einstein-gauss-bonnet theory. *Physical Review Letters* 106. URL: <http://dx.doi.org/10.1103/PhysRevLett.106.151104>, doi:10.1103/physrevlett.106.151104.
- Koh, S., Lee, B.H., Lee, W., Tumurtushaa, G., 2014. Observational constraints on slow-roll inflation coupled to a Gauss-Bonnet term. *Phys. Rev. D* 90, 063527. doi:10.1103/PhysRevD.90.063527, arXiv:1404.6096.
- Kokubu, T., Harada, T., 2020. Thin-shell wormholes in einstein and einstein-gauss-bonnet theories of gravity. *Universe* 6. URL: <https://www.mdpi.com/2218-1997/6/11/197>, doi:10.3390/universe6110197.
- Liang, Q., Sakstein, J., Trodden, M., 2019. Baryogenesis via gravitational spontaneous symmetry breaking. *Phys. Rev. D* 100, 063518. doi:10.1103/PhysRevD.100.063518, arXiv:1904.10510.
- Lyth, D.H., Stewart, E.D., 1992. The curvature perturbation in power-law (e.g. extended) inflation. *Physical Review D* 46, 532–538. URL: <http://dx.doi.org/10.1103/PhysRevD.46.532>, doi:10.1103/PhysRevD.46.532.
- Markkanen, T., Tranberg, A., 2019. The decoupling limit in the presence of a cosmological constant. *Physics Letters B* 793, 134830. URL: <http://dx.doi.org/10.1016/j.physletb.2019.134830>, doi:10.1016/j.physletb.2019.134830.
- Nikulin, V.V., Krasnov, M.A., Rubin, S.G., 2022. Compact extra dimensions as the source of primordial black holes. *Frontiers in Astronomy and Space Sciences* 9. URL: <https://www.frontiersin.org/journals/astronomy-and-space-sciences/articles/10.3389/fspas.2022.927144>, doi:10.3389/fspas.2022.927144.
- Nojiri, S., Odintsov, S.D., Oikonomou, V.K., 2019. Ghost-free gauss-bonnet theories of gravity. *Physical Review D* 99. URL: <http://dx.doi.org/10.1103/PhysRevD.99.044050>, doi:10.1103/physrevd.99.044050.
- Odintsov, S., Oikonomou, V., 2020. Swampland implications of gw170817-compatible einstein-gauss-bonnet gravity. *Physics Letters B* 805, 135437. URL: <http://dx.doi.org/10.1016/j.physletb.2020.135437>, doi:10.1016/j.physletb.2020.135437.
- Parker, L., Toms, D.J., 1985. New form for the coincidence limit of the feynman propagator, or heat kernel, in curved spacetime. *Physical Review D* 31, 953–957. URL: <http://dx.doi.org/10.1103/PhysRevD.31.953>, doi:10.1103/PhysRevD.31.953.
- Pinto, M.A.S., 2025. Λ CDM-like evolution in einstein-scalar-gauss-bonnet gravity. *The European Physical Journal C* 85. doi:<https://doi.org/10.1140/epjc/s10052-025-14796-5>.
- Planck Collaboration, Akrami, Y., 2020. Planck 2018 results - x. constraints on inflation. *Astronomy & Astrophysics* 641, A10. URL: <https://doi.org/10.1051/0004-6361/201833887>, doi:10.1051/0004-6361/201833887.
- Rashidi, N., Nozari, K., 2020. Gauss-Bonnet Inflation after Planck2018. *Astrophys. J.* 890, 58. doi:10.3847/1538-4357/ab6a10, arXiv:2001.07012.
- Sasakura, N., 2002. A de-sitter thick domain wall solution by elliptic functions. *Journal of High Energy Physics* 2002, 026. URL: <https://doi.org/10.1088/1126-6708/2002/02/026>, doi:10.1088/1126-6708/2002/02/026.
- Sher, M., 1989. Electroweak higgs potentials and vacuum stability. *Physics Reports* 179, 273–418. URL: [http://dx.doi.org/10.1016/0370-1573\(89\)90061-6](http://dx.doi.org/10.1016/0370-1573(89)90061-6), doi:10.1016/0370-1573(89)90061-6.
- Silva, H.O., Sakstein, J., Gualtieri, L., Sotiriou, T.P., Berti, E., 2018. Spontaneous scalarization of black holes and compact stars from a gauss-bonnet coupling. *Physical Review Letters* 120. URL: <http://dx.doi.org/10.1103/PhysRevLett.120.131104>, doi:10.1103/physrevlett.120.131104.
- Sotiriou, T.P., Zhou, S.Y., 2014. Black hole hair in generalized scalar-tensor gravity. *Physical Review Letters* 112. URL: <http://dx.doi.org/10.1103/PhysRevLett.112.251102>, doi:10.1103/physrevlett.112.251102.
- Weinberg, E.J., Wu, A., 1987. Understanding complex perturbative effective potentials. *Phys. Rev. D* 36, 2474–2480. URL: <https://link.aps.org/doi/10.1103/PhysRevD.36.2474>, doi:10.1103/PhysRevD.36.2474.
- Weinberg, S., 2005. Quantum contributions to cosmological correlations. *Physical Review D* 72, 043514. URL: <http://dx.doi.org/10.1103/PhysRevD.72.043514>, doi:10.1103/PhysRevD.72.043514.
- Yi, Z., Gong, Y., Sabir, M., 2018. Inflation with Gauss-Bonnet coupling. *Phys. Rev. D* 98, 083521. doi:10.1103/PhysRevD.98.083521, arXiv:1804.09116.
- Yogesh, Mohammadi, A., Wu, Q., Zhu, T., 2025. Starobinsky like inflation and egb gravity in the light of act. *Journal of Cosmology and Astroparticle Physics* 2025, 010. URL: <https://doi.org/10.1088/1475-7516/2025/10/010>, doi:10.1088/1475-7516/2025/10/010.
- Yousaf, M., Asad, H., Aslam, M., 2025. Implications of modified gauss-bonnet gravity on gravastar-like structures: High-energy stability and electromagnetic effects. *High Energy Density Physics* 57,

101221. URL: <https://www.sciencedirect.com/science/article/pii/S1574181825000497>,
doi:<https://doi.org/10.1016/j.hedp.2025.101221>.

Zahoor, M., Khan, S., Bhat, I.A., 2026. Reconciling fractional power potential and egb gravity in the light of act. *Journal of High Energy Astrophysics* 49, 100458.
URL: <https://www.sciencedirect.com/science/article/pii/S2214404825001399>, doi:<https://doi.org/10.1016/j.jheap.2025.100458>.